Finite Elements for Thermoelectric Device Analysis in ANSYS

Elena E. Antonova and David C. Looman
ANSYS Inc.
Southpointe, Technology Drive, Canonsburg, PA 15317, USA

Abstract

A new set of ANSYS coupled-field elements enables users to accurately and efficiently analyze thermoelectric devices. This paper reviews the finite element formulation, which, in addition to Joule heating, includes Seebeck, Peltier, and Thomson effects. Examples of steady-state and transient simulations of a thermoelectric generator and a single-stage Peltier cooler are presented for thermoelectric analysis verification. An analysis of a multistage thermoelectric cooler is performed to demonstrate ANSYS parametric analysis capability.

1. Introduction

The finite element method (FEM) has become an essential solution technique in many areas of engineering and physics. The FEM versatility lies in its ability to model arbitrary shaped structures, work with complex materials, and apply various types of loading and boundary conditions. The method can easily be adapted to different sets of constitutive equations, which makes it particularly attractive for coupled-physics simulation.

The ANSYS finite element program has a large library of elements that support structural, thermal, fluid, acoustic, and electromagnetic analyses, as well as coupled-field elements that simulate the interaction between the above fields. Examples of ANSYS coupled-physics capabilities include thermal-structural, fluid-structure, electromagnetic-thermal, thermal-electric, structural-thermal-electric, piezoelectric, piezoresistive, magneto-structural, and electrostatic-structural analyses [1].

Until recently, the ANSYS thermal-electric analysis only accounted for the Joule heat as a coupling mechanism between the thermal and electric fields. However, over the past few years, there has been an increase in the number of requests for the simulation of thermoelectric devices for applications such as electronic and optical component cooling, MEMS, thermal energy harvesting and many others, which require modeling the Seebeck and Peltier effects. While simple one-dimensional analytical models are frequently being used to predict the performance of such devices [2], the diversity and complexity of thermoelectric applications typically necessitates a full three-dimensional (3-D) numerical analysis.

To answer these needs, the thermal-electric analysis has been enhanced in ANSYS 9.0 to incorporate the above effects. In the following sections, a general 3-D finite element formulation is introduced and illustrated by several numerical examples.

2. Governing Equations of Thermoelectricity

In a thermoelectric analysis the equations of heat flow

$$\rho C \frac{\partial T}{\partial t} + \nabla \cdot \mathbf{q} = \dot{q} \qquad (1)$$

and of continuity of electric charge

$$\nabla \cdot \left(\mathbf{J} + \frac{\partial \mathbf{D}}{\partial t} \right) = 0 \qquad (2)$$

are coupled by the set of thermoelectric constitutive equations [3]

$$\mathbf{q} = [\Pi] \cdot \mathbf{J} - [\lambda] \cdot \nabla T, \qquad (3)$$

$$\mathbf{J} = [\sigma] \cdot (\mathbf{E} - [\alpha] \cdot \nabla T) \qquad (4)$$

and the constitutive equation for a dielectric medium

$$\mathbf{D} = [\varepsilon] \cdot \mathbf{E}, \qquad (5)$$

where:

ρ = density, kg/m^3,

C = specific heat capacity, J/(kg - K),

T = absolute temperature, K,

$\dot{q}$ = heat generation rate per unit volume, W/m^3,

$\mathbf{q}$ = heat flux vector, W/m^2,

$\mathbf{J}$ = electric current density vector, A/m^2,

$\mathbf{E}$ = electric field intensity vector, V/m,

$\mathbf{D}$ = electric flux density vector, C/m^2,

$[\lambda]$ = thermal conductivity matrix, W/m - K,

$[\sigma]$ = electrical conductivity matrix, S/m,

$[\alpha]$ = Seebeck coefficient matrix, V/K,

$[\Pi] = T[\alpha]$ = Peltier coefficient matrix, V,

$[\varepsilon]$ = dielectric permittivity matrix, F/m.

In the absence of time-varying magnetic fields, the electric field $\mathbf{E}$ is irrotational $(\nabla \times \mathbf{E} = 0)$, and can be derived from an electric scalar potential φ:

$$\mathbf{E} = -\nabla \varphi. \qquad (6)$$

Substituting Eqs. (3)-(6) into Eqs. (1)-(2) produces a system of coupled equations of thermoelectricity:

$$\rho C \frac{\partial T}{\partial t} + \nabla \cdot ([\Pi] \cdot \mathbf{J}) - \nabla \cdot ([\lambda] \cdot \nabla T) = \dot{q}, \qquad (7)$$

$$\nabla \cdot \left([\varepsilon] \cdot \nabla \frac{\partial \varphi}{\partial t} \right) + \nabla \cdot ([\sigma] \cdot [\alpha] \cdot \nabla T) + \nabla \cdot ([\sigma] \cdot \nabla \varphi) = 0, \qquad (8)$$

where the heat generation term $\dot{q}$ in Eq. (7) includes electric power $\mathbf{J} \cdot \mathbf{E}$ spent on Joule heating and on work against the Seebeck field $[\alpha] \nabla T$.

Note that the displacement current $\frac{\partial \mathbf{D}}{\partial t}$ associated with the capacitive effects has been included in the system of equations for completeness, even though it may not play a significant role in thermoelectric applications unless fast transient processes are considered.

3. Finite Element Formulation

The system of thermoelectric finite element equations can be obtained by applying the Galerkin FEM procedure [4] to the coupled equations derived in the previous section. This technique involves (a) approximating the temperature T and electric scalar potential φ over a finite element as:

$$T = \mathbf{N} \cdot \mathbf{T}_e, \tag{9}$$

$$\varphi = \mathbf{N} \cdot \varphi_e, \tag{10}$$

where:

$\mathbf{N}$ = vector of element shapes functions,

$\mathbf{T}_e$ = vector of nodal temperatures,

φ_e = vector of nodal electric potentials,

(b) writing the system of Eqs. (7) and (8) in a weak projective form, (c) integrating the projective equations by parts, and (d) taking into account the Neumann boundary conditions. Without further elaboration, the resulting system of thermoelectric finite element equations is:

$$\begin{bmatrix} C^{TT} & 0 \\ 0 & C^{\varphi\varphi} \end{bmatrix} \begin{Bmatrix} \dot{T}_e \\ \dot{\varphi}_e \end{Bmatrix} + \begin{bmatrix} K^{TT} & 0 \\ K^{\varphi T} & K^{\varphi\varphi} \end{bmatrix} \begin{Bmatrix} T_e \\ \varphi_e \end{Bmatrix} = \begin{Bmatrix} Q + Q^P + Q^e \\ I \end{Bmatrix}, \tag{11}$$

where the element matrices and load vectors are obtained by numerical integration (using Gauss quadratures) over the element volume V:

$K^{TT} = \int_V \nabla \mathbf{N} \cdot [\lambda] \cdot \nabla \mathbf{N} dV$ - thermal stiffness matrix,

$K^{\varphi\varphi} = \int_V \nabla \mathbf{N} \cdot [\sigma] \cdot \nabla \mathbf{N} dV$ - electric stiffness matrix,

$K^{\varphi T} = \int_V \nabla \mathbf{N} \cdot [\sigma] \cdot [\alpha] \cdot \nabla \mathbf{N} dV$ - Seebeck stiffness matrix,

$C^{TT} = \rho \int_V C \mathbf{N} \mathbf{N} dV$ - thermal damping matrix,

$C^{\varphi\varphi} = \int_V \nabla \mathbf{N} \cdot [\varepsilon] \cdot \nabla \mathbf{N} dV$ - dielectric damping matrix,

Q - vector of combined heat generation loads,

$Q^P = \int_V \nabla \mathbf{N} \cdot [\Pi] \cdot \mathbf{J} dV$ - Peltier heat load vector,

$Q^e = \int_V \mathbf{N} \mathbf{E} \cdot \mathbf{J} dV$ - electric power load vector,
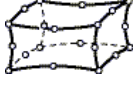
I - electric current load vector.

Thermal loads (Q) can be in the form of imposed temperature, point heat flow rate, surface heat flux, convection, or radiation, as well as body heat generation rate for causes other than electric power dissipation (accounted for in Q^e). Electrical loads (I) can be in the form of imposed electric potential and point electric current. Linear electric circuit components (resistors, capacitors, and voltage or current sources) can be connected to the finite element model to simulate passive and active electrical loads.

The ANSYS input of material matrices $[\lambda]$, $[\sigma]$, $[\alpha]$, $[\varepsilon]$ is in the form of their diagonal terms, i.e. material coefficients along the x, y, z axes. This input can be combined with an arbitrarily oriented element coordinate system to account for an alternative material orientation. Electrical properties are input as resistivity and internally converted into conductivity $[\sigma]$, which is the conductivity evaluated at zero temperature gradient $(\nabla T = 0)$. The input $[\lambda]$ is the thermal conductivity evaluated at zero electric current $(\mathbf{J} = 0)$. All material properties can be temperature dependent. In particular, Thomson effect is taken into account by specifying temperature dependent Seebeck coefficients $[\alpha]$.

The analysis is supported by three isoparametric coupled-field elements with structural, thermal, and electrical degrees of freedom at nodes (Table 1). The 8-node quadrilateral allows degeneration into a 6-node triangle, and, in addition to a 2-D plane behavior that assumes a unit thickness, it can model 3-D axisymmetric geometries. The 3-D 20-node hexahedron ('brick' element) can be degenerated into a 10-node tetrahedron, a 13-node pyramid, or a 15-node prism.

Table 1: Finite elements for a thermoelectric analysis

PLANE223		2-D 8-node quadrilateral
SOLID226		3-D 20-node hexahedron
SOLID227		3-D 10-node tetrahedron

The global matrix equation is assembled from the individual finite element equations, and is non-symmetric like Eq. (11). Since the thermal load vector depends on the electric solution, the analysis is non-linear (steady-state or time-transient) and requires at least two iterations to converge. The temperature offset from zero to absolute zero should be specified if temperature is in units other than kelvins.

The solution yields temperatures (T_e) and electric potentials (φ_e) at unconstrained nodes, or reactions in the form of heat flow rate and electric current at nodes with imposed temperature and electric potential respectively. The temperature gradient and electric field are calculated as

$$\nabla T = \nabla \mathbf{N} \cdot T_e, \tag{12}$$

$$\mathbf{E} = -\nabla \mathbf{N} \cdot \varphi_e, \tag{13}$$

and then substituted into Eqs. (3)-(5) to obtain the values of $\mathbf{J}$, $\mathbf{q}$, $\mathbf{D}$ fields, and Joule heat generation density for each element. To determine the deformation and stress distribution in the device due to thermal expansion, the same coupled-field elements can be used to perform a structural-thermal-electric analysis that solves for the displacement, temperature and electric potential fields simultaneously.

4. Steady-State Analysis of a Thermoelectric Generator

This example considers the performance of a thermoelectric generator described in Angrist [2]. The generator (Fig.1) operates between $T_c = 27°C$ and $T_h = 327°C$. The element length is $L_p = L_n = 1\,\text{cm}$ for both the p-type and n-type semiconductors, and the element cross-sectional areas are $A_p = 1.24\,\text{cm}^2$ and $A_n = 1\,\text{cm}^2$ respectively. The cold sides of the element are connected to a load resistance $R_o = 3.92 \times 10^{-3}\,\Omega$.
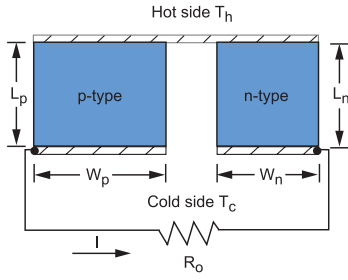
Figure 1: Thermoelectric generator.

Two steady-state analyses using SOLID226 were performed to determine the heat input Q_h, the power output P_o, the thermal efficiency $\eta = P_o/Q_h$, and the electric current I. The material properties for n- and p-type bismuth telluride alloys used in the simulation can be found in [2]. The first analysis (a) uses the material properties evaluated at average temperature of 177°C, while the second analysis (b) uses the temperature dependent electrical resistivity, thermal conductivity, and Seebeck coefficient. Computed and analytical parameters of the generator are summarized in Table 2.

Table 2: Comparison of generator parameters

Quantity	Reference [2]	ANSYS (a)	ANSYS (b)
Q_h, W	13.04	13.03	11.07
P_o, W	1.44	1.43	1.05
η, %	11.0	11.0	9.5
I, A	19.2	19.1	16.4

Numerical results from the first analysis match the theoretical design [2]. In the second, more realistic, analysis, the thermal efficiency is reduced by 15% as a result of taking into account the temperature dependence of material properties.

5. Steady-State Analysis of a Single-Stage Peltier Cooler

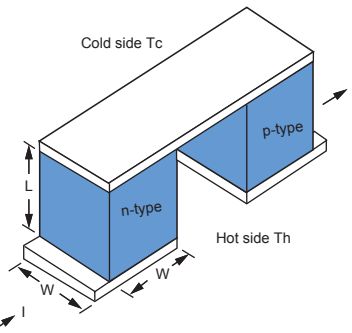This example considers the performance of a thermoelectric cooler (Fig. 2).

Figure 2: Thermoelectric cooler.

The cooler, composed of two semiconductor elements of size $L = W = 1$ cm electrically connected at the cold junction by a copper strap, maintains the cold side at $T_c = 0°C$ and dissipates heat from the hot junction at $T_h = 54°C$ on the passage of the electric current of magnitude $I = 28.7$ A.

A steady-state analysis was performed using a combination of SOLID226 and SOLID227 elements to mesh the cooler model. The material properties for the analysis were evaluated at the average cooler temperature of 27°C. The calculated temperature distribution in the cooler is shown in Fig. 3.
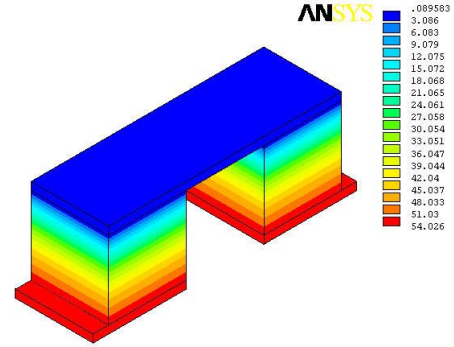

Figure 3: Temperature distribution in the cooler.

The coefficient of performance was determined as $\beta = Q_c/P_i$, where Q_c is the rate at which heat is removed from the cold junction, and P_i is the power input to the cooler. Q_c is obtained as the total heat flow rate reaction at the cold junction nodes with imposed temperature constrain T_c; the power input P_i is calculated from the electric current load I and the voltage drop between the hot junction electrodes. The value of $\beta = 0.32$ was obtained with both the ANSYS simulation and the analytical design [2].

6. Transient Analysis of a Single-Stage Peltier Cooler

This example considers a time-transient response of a Peltier cooler to a current pulse excitation. The cooler, experimentally investigated by Snyder *et al*. [5], consists of two $1 \text{ mm} \times 1 \text{ mm} \times 5.8 \text{ mm}$ thermoelectric elements with cold junctions soldered by a 35 μm thick copper foil. A square current pulse of a magnitude 2.5 times higher than the steady-state current $I_s = 0.675$ A (Fig. 4) is applied to the cooler to achieve a temporary supercooling of the cold junction.
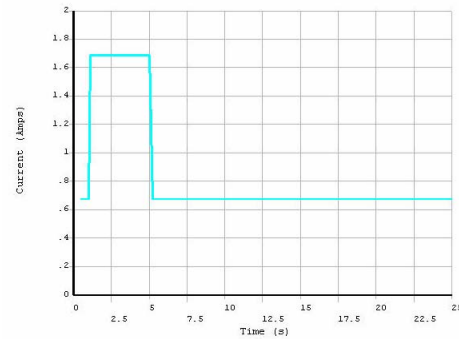

Figure 4: Current load vs. time.

A transient thermoelectric analysis was performed to determine the temperature of the cold junction as a function of time. The material properties used in the simulation are summarized in Table 3.

Table 3: Material properties

Material Property	Bi_2Te_3	Copper
σ, S/m	1.1×10^5	5.9×10^8
k, W/ K-m	1.6	350
α, V/K	$\pm 200 \times 10^{-6}$	6.5×10^{-6}
C, J/K-kg	154.4	385
ρ, kg/ m^3	7740	8920

A convection boundary condition with a film coefficient of $h = 3 \text{ W/K} \cdot \text{m}^2$ was applied to all the surfaces of the cooler except for the hot ends. Although fitting the experimental curve reported in [5] was not the purpose of the present example, the calculated cold side temperature (Fig. 5) shows a good agreement with the experimental transient behavior of the cooler in terms of the lowest temperature achieved, the post-pulse highest temperature, and the time to return to the steady-state.
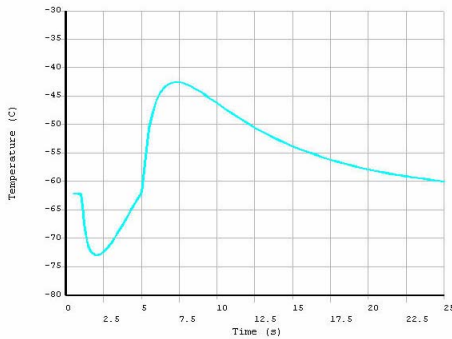

Figure 5: Temperature of cold junction vs. time

7. Parametric Analysis of a Multi-Stage Peltier Cooler

In ANSYS, input and output quantities such as dimensions, material properties, loads, temperature and voltage results, heat flux, and stress can be varied parametrically. Tools are available for design optimization and statistical analysis of parametric results. For example, in the analysis of a thermoelectric device, cold-side temperature can be minimized as a function of the Peltier block height and the input current, subject to a limit on the maximum stress.

In the following example, the ANSYS Workbench™ interface was used to create and analyze a thermoelectric cooler similar in size and construction to those used in commercial applications. Workbench provides two-way parametric associativity with most CAD programs as well as its internal solid modeling tool Design Modeler, which was used in this study. A number of *n*-type and *p*-type Peltier blocks are electrically connected in series between two ceramic plates (Fig. 6). The height of the Peltier blocks and the applied current were parameterized. Taller heights increase the Joule heat in the blocks due to greater electrical resistance. For some heights the Joule heat completely nullified the Peltier cooling. Shorter heights increase thermal conduction between the hot and cold sides. The current

increases both the cooling and Joule heating. The response surface for the cold side of the cooler is shown in Fig. 7.
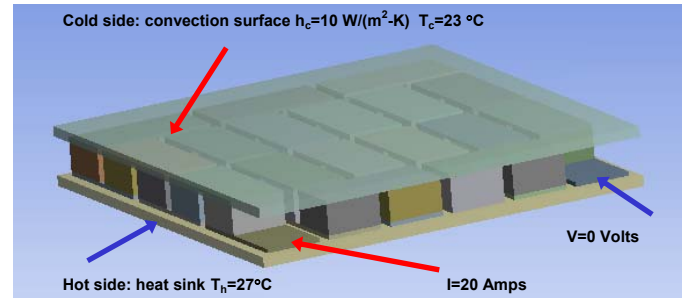

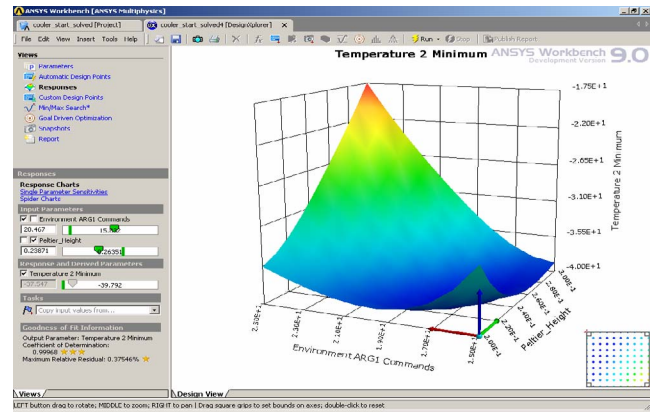**Figure 6:** Multi-stage cooler model.

Figure 7: Response surface for the cold side temperature.

Conclusions

A new set of ANSYS coupled-field elements enables users to accurately and efficiently analyze thermoelectric devices. The steady-state, time-transient and parametric simulations of various thermoelectric applications have been performed to demonstrate the new capability. Numerical results agree with the device performance predicted by analytical models and experimental data. It is hoped that the new tool will find applications in the design and simulation of thermoelectric devices.

References

1. ANSYS Release 9.0 Documentation (2004)
2. Angrist, S. W., Direct Energy Conversion, 3rd Edition, Allyn and Bacon (Boston, 1976), pp. 140-166.
3. Landau L. D. and Lifshitz, E. M., Electrodynamics of Continuous Media, 2nd Edition, Butterworth-Heinemann (Oxford, 1984)
4. Silvester P. P. and Ferrari, R. L., Finite Elements for Electrical Engineers, 3rd Edition, University Press (Cambridge, 1996)
5. Snyder, G. J. et al, "Supercooling of Peltier cooler using a current pulse," *J. Appl. Phys*, Vol. 2, No. 3 (2002), pp. 1564-1569.